J Mater Sci

Materials for life sciences

Laser-induced surface texturing and nanomaterial functionalization of PLA/PHBV surfaces for enhanced cell adhesion

Rafaela Campos Queiroz[1], Vanessa Modelski Schatkoski[1], Rodrigo Luiz Moraes Saldanha Oliveira[1], Yannic Sterzl[2], Alexandra Reif[2], Heino Besser[2], Simone Weigel[3], Tim Scharnweber[3], Ana Paula Lemes[1], Carolina Ramos Hurtado[4], Wilhelm Pfleging[2,*], and Dayane Batista Tada[1,*]

[1] *Institute of Science and Technology, Federal University of São Paulo (UNIFESP), São José dos Campos, Brazil*
[2] *Institute for Applied Materials-Applied Materials Physics (IAM-AWP), Karlsruhe Institute of Technology, Karlsruhe, Germany*
[3] *Institute for Biological Interfaces (IBG 1), Karlsruhe Institute of Technology, Karlsruhe, Germany*
[4] *Federal Institute of São Paulo, São José dos Campos, Brazil*

Received: 25 February 2026
Accepted: 7 August 2026

ABSTRACT

Current research on the development of biomaterials aims at reducing bacterial colonization and increasing cell adhesion on the surface of implantable devices for regenerative medicine. Equally noteworthy is the growing interest in using materials from renewable sources and biodegradable in medical devices. In this study, femtosecond laser surface texturing was applied to PLA/PHBV polymer blends nanocomposites with and without cellulose nanocrystals (CNCs) and carbon nanotubes (CNTs) fillings. Micro-pillar structures were developed using a femtosecond laser. The textured samples were characterized by SEM, profilometry, and contact angle measurements. The effect of texturing on cytotoxicity, cell adhesion and proliferation were evaluated by MTT assay and confocal fluorescence microscopy by using L929 fibroblasts cell line. The results showed that laser texturing led to a significant increase in surface roughness and caused the material to change from hydrophilic to hydrophobic behavior, a phenomenon explained by the Wenzel model. The polymers showed higher cell viability and directional growth after laser treatment, especially in the samples containing 0.5–1.5 wt% CNT and up to 5 wt% CNC. However, it was observed that at high concentrations of nanofillers the biocompatibility was compromised, which could be attributed to particle agglomeration and percolation effects. Overall, this study highlights the synergistic role of laser-induced microstructures and functionalization with nanomaterials in modulating the surface properties of biopolymers to promote biocompatibility, offering a promising approach for the development of bioactive surfaces for high-performance implants.

Handling Editor: Maude Jimenez.

Address correspondence to E-mail: wilhelm.pfleging@kit.edu; d.tada@unifesp.br

https://doi.org/10.1007/s10853-026-13569-z

Springer

Published online: 22 August 2026

Introduction

One of the main problems encountered with implantable medical devices is bacterial adhesion, which leads to implant-related infections. However, the improvement of implant surfaces has been increasingly explored, with a view to offering better quality of life and prolonged life expectancy to the patient [1]. Infections caused by implants are responsible for prolonged hospital stays, high healthcare costs, the need for multiple revision surgeries, and significant patient morbidity. Recent studies [2] estimate that post-operative infection rates following orthopedic procedures involving internal devices are approximately 5%. In such cases, hospital expenses are reported to be up to eight times higher compared to surgeries without fracture-related infections. Consequently, research has focused on enhancing implant surface properties to reduce the risk of infection.

The surface properties of biomedical implants are closely linked to their functionality. Key factors such as chemical composition, surface topography, and mechanical characteristics play a critical role in either inhibiting or promoting bacterial proliferation during the initial phase, as well as in biofilm formation. These properties also significantly influence tissue healing [3]. Femtosecond laser texturing has stood out among surface modification techniques due to its ability to precisely design micro-and nanoscale structures without causing significant thermal damage to the materials [4]. Micro-patterning using femtosecond laser-induced pillar structures, for example, has shown promise in increasing cell adhesion and proliferation and, at the same time, offers potential benefits in reducing bacterial colonization due to the increase in surface roughness and topographical characteristics [5]. Also, it has been shown that grooved and pillar-like textures guide cell alignment and increase the surface area for anchoring, promoting adhesion and proliferation, while at the same time creating unfavorable conditions for bacterial colonization, disrupting biofilm formation [1]. The dual functionality of these surface patterns makes femtosecond laser structuring a promising tool in the development of antibacterial and bioactive implants.

Polylactic acid (PLA) and poly(3-hydroxybutyrate-co-3-hydroxyvalerate) (PHBV) are biopolymers widely used in biomedical applications due to their biodegradability, biocompatibility, and favorable mechanical properties [6]. PLA and PHBV are increasingly gaining traction as an alternative to traditional biomedical implants. Despite the fact that both PLA and PHBV are biodegradable, in terms of natural sources, PHBV has an advantage over PLA since PLA is synthetic. Although metals offer mechanical strength and durability, they generally lack resorption capacity and can trigger adverse immune responses or long-term complications. Biopolymers, on the other hand, offer temporary support and are gradually resorbed by the body, eliminating the need for secondary surgery to remove the implant and reducing chronic inflammatory reactions. These attributes make them particularly attractive for use in regenerative medicine and temporary implantable devices [6]. Currently, the wider clinical use of these materials encounters barriers due to their inherent fragility and hydrophobicity.

Therefore, integrating these polymers with nanomaterials, such as cellulose nanocrystals (CNCs) and carbon nanotubes (CNTs), has been investigated as a promising strategy to overcome these limitations, significantly increasing mechanical strength, stiffness, and biological interactions. Specifically, CNTs present exceptional mechanical reinforcement capabilities, increase cell adhesion and proliferation, while CNCs offer biocompatibility, biodegradability, and customizable surface functionalities that promote favorable cell interactions [7–9]. Among the benefits of CNTs are their exceptional mechanical reinforcement capabilities, which lead to an increase in the tensile strength and modulus of elasticity of polymers, making them essential in the application of load-bearing implants. Their electrical properties and high surface area also facilitate improved cell interactions, favoring cell adhesion and proliferation [7]. As for the benefits of CNCs, it is possible to highlight not only the provision of mechanical reinforcement, but also the significant improvement in the hydrophilicity of PLA and PHBV compounds, directly influencing biological responses, promoting the uniform distribution of cells on the implant surface, and improving biocompatibility [8]. The integration of these nanomaterials into PLA/PHBV blends, combined with precise surface texturing with femtosecond lasers, presents a sophisticated strategy for the development of state-of-the-art biomedical implants capable of significantly reducing bacterial adhesion and, at the same time, promoting effective tissue integration [9].

Although progress has been made in research within this field, significant gaps remain—particularly regarding the optimal integration of nanomaterials into polymer matrices and the comprehensive understanding of how nanomaterial incorporation combined with laser-induced surface modifications affects biological interactions. The present study addresses these gaps by exploring the combined impact of femtosecond laser-induced surface texturing and nanomaterial functionalization with CNCs and CNTs on PLA/PHBV blends. By systematically evaluating cell adhesion, proliferation, and viability on these engineered surfaces, this work aims to promote the development of new biomaterials designed to improve clinical outcomes by reducing bacterial colonization and promoting superior tissue integration.

Experiments section

Preparation of polymer samples

The samples investigated in this study comprised pure PHBV; PHBV containing different concentrations of cellulose nanocrystals (CNC); PLA/PHBV blends with varying compositions; and PLA/PHBV (80:20) composites containing different concentrations of carbon nanotubes (CNT), as detailed in Table 1. All the samples were cut to 13x10mm using Precision Cutoff Machine Brilliant 220 (QATM), and then the surface of all samples was polished.

Table 1 Composition of the samples investigated in this study

Sample	Composition
PHBV	Pure PHBV
PHBV with CNC	PHBV + 1 wt% CNC
	PHBV + 3 wt% CNC
	PHBV + 5 wt% CNC
	PHBV + 10 wt% CNC
PLA/PHBV blends	PLA/PHBV blend (50:50)
	PLA/PHBV blend (60:40)
	PLA/PHBV blend (70:30)
	PLA/PHBV blend (90:10)
PLA	Pure PLA
PLA/PHBV 80:20 with CNT	PLA/PHBV (80:20) + 0.5 wt% CNT
	PLA/PHBV (80:20) + 1 wt% CNT
	PLA/PHBV (80:20) + 1.5 wt% CNT
	PLA/PHBV (80:20) + 2 wt% CNT

Preparation of PHBV samples using CNC

CNC incorporation was performed exclusively in the PHBV matrix since one of the goals of this work was to explore a material composed of a matrix and nanofillers both derived from renewable sources, obtained through natural processes and fully biodegradable. It is important to note that although PLA is a biodegradable polymer, it has a synthetic origin. Therefore, PHBV matrix containing CNC would result would have an advantage of being completely from natural source over the PLA/PHBV composite.

First, the pure PHBV pellets were dried in an oven (Solab, SL-100) for 24 hours at 70 °C. Next, the solvent evaporation method was used to incorporate the CNC onto the surface of the pellets. Acetone was chosen as the solvent due to its low boiling point and its inability to dissolve PHBV.

A CNC suspension was prepared in acetone using the Sonics Vibra-cell VCX750 ultrasonic processor for 2 minutes at 45% amplitude. The resulting suspension was then dispensed onto the PHBV pellets, and the sample was dried in an oven, where the acetone evaporated. Finally, the mixture was placed in the thermokinetic mixer chamber (MH Equipamentos, MH-50H) at a speed of 3000 rpm for 14 seconds. It is important to note that the mixer has a maximum permitted mass of 65 g, so the masses used vary according to the CNC percentage for each case (1, 3, 5, and 10%).

Finally, compression molding was performed using a hydropneumatic press (MH Equipamentos, RP8HP, maximum load: 8 tons). Molding took place at 200 °C over three cycles: molding at 2 tons for 2 minutes, molding at 8 tons for 1.5 minutes, and finally, cooling for 2 minutes at 2 tons.

Preparation of PLA/PHBV blends with and without CNTs

The polymer blends were processed by extrusion. To do this, the polymers were first dried in a vacuum oven for 4 hours at 70 °C.

A mini twin-screw extruder (AX Plásticos, AX16:40DR) was used. A total of 400 g of material was processed at 165–170 °C, with a rotation speed of 100 rpm and a feed rate of 30 rpm. After extrusion, the material was pelletized, and PLA/PHBV blends with and without CNTs were obtained.

It is important to note that the 80:20 PLA/PHBV blend was selected for CNT incorporation based on previous evidence in the literature showing that this ratio offers a favorable balance between processability and toughness compared to other PLA/PHBV blends. Previous studies [10, 11, 12] reported that the addition of 20% PHBV to PLA promotes a significant increase in ductility and impact resistance, making this composition particularly attractive for biomedical applications. Therefore, the present study adopted the 80:20 composition as a reference matrix to specifically evaluate the effects of CNT incorporation and laser texturing on the material's biological properties.

Laser structure

The laser pillar structure was made on top of each polymer sample using an ultrafast femtosecond fiber laser (Tangerine, Amplitude Systèmes). The pillars were built at a distance of 30x30μm (grid), using a wavelength of 515nm, 200KHz, at a power of 0.68W, at a speed of 800mm.s^{-1}, 360 fs, and two repetitions each. The texturing was then verified using scanning electron microscopy and optical microscopy. The laser pillar structure was made on top of all the samples described in Table 1.

Topography measurements

The topography of the material after laser texturing was measured using a Keyence VHX-7000 digital microscope, using the focus variation method. The height and the distance between the pillars were measured, transversely and longitudinally. The optical properties of the materials directly influenced the results of the topography measurements; and therefore, it was only possible to obtain these data for the four samples containing CNTs (PLA/PHBV 80:20 + 0.5, 1, 1.5 and 2 wt% CNT).

Contact angle measurement

The contact angle was measured using the Microdrop MD-E-3000 device using a sessile drop method and deionized water as a probe liquid. The deposition parameters were adjusted to ensure the formation of reproducible droplets, and a volume of 3 μL was set. A drop of deionized water was deposited gently on the surface of the sample. The equipment captured images of the interaction between the drop and the surface using a high-resolution optical system. The images were processed using the integrated software, which analyzed the profile of the drop and determined the contact angle by adjusting appropriate mathematical models. The procedure was repeated at different points on the surface to assess the homogeneity of the material's wettability.

The contact angle values were obtained automatically by the Microdrop MD-E-3000 software. The average of the measurements was calculated and compared between the different samples analyzed. The interpretation of the results considered the hydrophobicity or hydrophilicity of the material based on the angles obtained. All samples described in Table 1 were included in this analysis, with the exception of PHBV 3 wt% CNC, which was excluded because an insufficient amount of material was available for testing.

Cell viability test

Cell viability was assessed using the 3-(4,5-dimethylthiazol-2-yl)-2,5-diphenyltetrazolium bromide (MTT) assay. The samples were first sterilized with ethanol, then placed in a 12-well plate, and finally, L929 cells were cultured on the samples for 24h (12 x 10^4 cells/well), following the guidelines of ISO 10993-5:2009. The cells were grown in Eagle's Minimum Essential Medium (EMEM) culture medium with L-Glutamine, from American Type Culture Collection (ATCC), prepared with 1% penicillin and 10% fetal bovine serum.

After incubation, the entire volume of each well was removed. The samples were washed once by carefully adding and removing phosphate-buffered saline (PBS). With the light off, MTT solution at a concentration of 0.5 mg/mL was added to each well, and the plate was incubated for 3 hours at 37 °C and 5% CO_2.

After this period, the contents of each well were removed and pure dimethyl sulfoxide (DMSO) was added to dissolve the purple formazan in the cells. The liquid was transferred to a 96-well plate, and the plate was taken to read the absorbance of the plates at 540 nm on the plate reader BioTek Synergy™ HTX. All samples described in Table 1 were included in this analysis, with the exception of PHBV 3 wt% CNC, which was excluded because an insufficient amount of material was available for testing.

Cell viabilities were compared to each other using the following strategies. In order to evaluate the effect of laser texturing, cell viability was expressed as a ratio relative to each non-textured sample (set at 100%). In this analysis, each group was compared against this fixed reference value using a one-sample Student's t-test, with the resulting p values likewise adjusted using the Bonferroni correction. In order to evaluate the different composition of samples, each sample group was compared with the cells grown in the absence of sample, which was considered as 100% of cell viability. The values of cell viability among samples were evaluated by one-way analysis of variance (ANOVA); each formulation was then compared individually against the control well using a t test based on the pooled within-group variance obtained from the ANOVA, with the resulting p values adjusted for multiple comparisons within each panel using the Bonferroni correction. In both cases, all conditions were tested in triplicate (n = 3), and differences were considered statistically significant when $p < 0.05$.

Fluorescence confocal microscopy

Confocal microscopy images were taken using a ZEISS LSM 880. For that, the samples were first sterilized with ethanol, then placed in the 12-well plate and finally, L929 cells were cultured on the samples for 24h and 48h, respectively (12 x10^4 cells/well). The cells are grown in EMEM culture medium with L-Glutamine, from the ATCC brand, prepared with 1% penicillin and 10% fetal bovine serum.

After incubation, the cell culture medium was removed and the wells were washed three times with PBS. Then 2 mL of 4% formaldehyde (diluted in PBS) was added, and the sample was left to stand for 20 minutes. After this period, the formaldehyde was removed and the samples were washed three times with PBS. Then, 2 mL of 0.1% Triton diluted in PBS was added to each well. After 4 minutes, the solution was removed and the well with the samples was washed again three times with PBS. Then, 2 mL of albumin (Albumin BSA Fraction V, PanReac AppliChem ITW Reagents) 1% diluted in PBS was added to each well. After 15 minutes, the solution was removed and the wells were washed again three times with PBS. 100 µL of phalloidin labeled with Alexa 488 (Alexa Fluor™ 488 Phalloidin, Invitrogen, ThermoFisher) was added to each well. The phalloidin was previously diluted in PBS (2 µL for 800 µL of PBS). The plate was wrapped in aluminum foil and left for 20 minutes. After this period, the phalloidin was removed and the samples were washed again three times with PBS. Then 100µL of DAPI (300 nM, Thermo Scientific) was added to each well and the samples were left for 5 minutes. Finally, the well was washed again three times with PBS and 5 µL of Invitrogen's ProLong Diamond Antifade Mountant was added between the sample and the glass coverslip, and the samples were stored at –20 °C. Confocal microscopy images were taken for all the samples described in Table 1.

Results and discussions

Laser structure

A laser ablation technique was used to build a pillar-like structure on the surface of the polymers [13]. Once the technique had been carried out, the resulting structures were verified by SEM, as shown in Fig. 1, on the PLA/PHBV 90:10 sample. This structure shown in the SEM was exactly the same for all samples.

Micro-pillars are generally produced in cross-line strategies [14]. In this study, the pillars were built at a distance of 30x30µm. The main advantage of using this technique was to increase the surface area of the material and consequently improve cell attachment on the surface.

Topography measurements

A three-dimensional micrograph of the PLA/PHBV 80:20 1.5% CNT sample is shown in Fig. 2. Information about the surface height is provided by the height profiles, where the colors vary according to height or depth. Additionally, a horizontal line was drawn across the surface of the samples, and the height and width profiles of the pillars were measured. The same procedure was followed when a vertical line was drawn. Figures 3 and 4 display these measurements for the laser-textured PLA/PHBV 80:20 0.5% CNT sample, followed by Table 2, which summarizes the measurements of all the CNT-containing samples.

Table 2 shows that in the samples with 0.5% CNT the average height and width of the pillars remain relatively close, with variations within the expected range. However, with the increase in CNT concentration, there is a tendency for greater variation in the measurements, especially in the vertical orientation. This is evidenced by the higher standard deviations in some conditions, such as in the sample with 1%

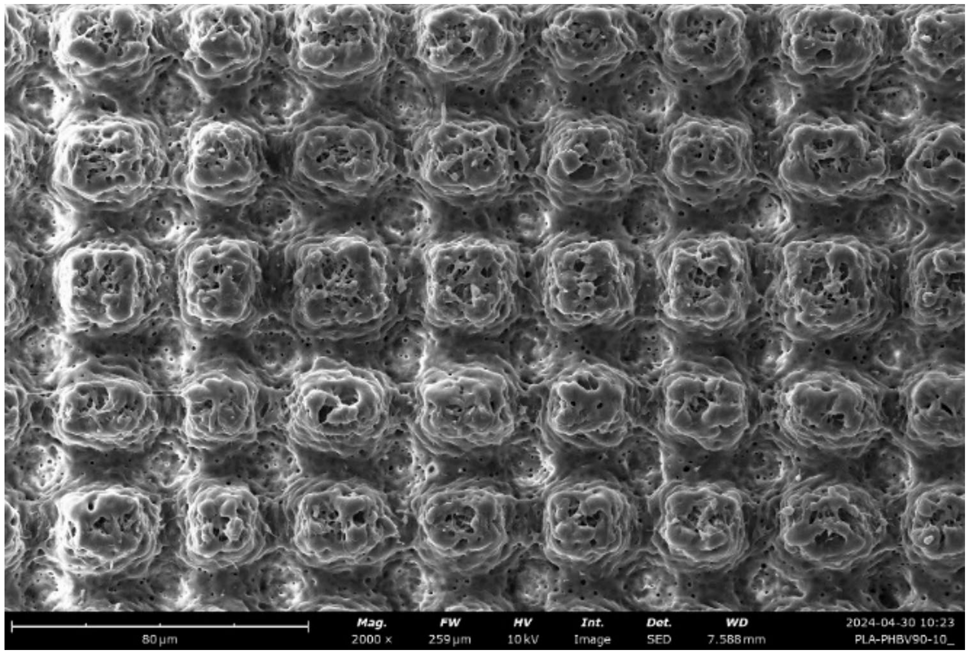

Figure 1 SEM of the PLA/PHBV 90:10 sample after texturing using a femtosecond laser (2000x).

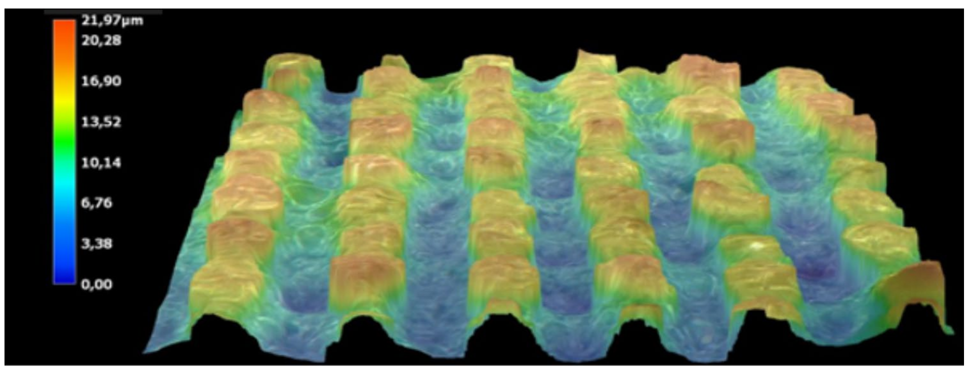

Figure 2 Three-dimensional micrograph of the laser-textured PLA/PHBV 80:20 1.5% CNT sample, showing the different heights of the pillars.

vertical CNT, where the height standard deviation reaches 2.47 µm.

Another relevant point is the impossibility of measuring the samples between 1.5 and 2% CNT in the horizontal orientation. The images obtained by optical profilometry provide relevant information on the morphology of the structures and are shown in Fig. 5.

These samples in Fig. 5 showed a highly irregular morphology, with great variation in the height of the structures. This irregularity made it difficult to clearly define the contours of the pillars, making it impossible to obtain consistent measurements. The comparison between the 1.5% and 2% horizontal CNT samples indicates that increasing the CNT concentration alters the interaction of the laser with the sample, which consequently alters the expected topographical patterns. This suggests that there is a limit to the CNT concentration that allows the structures to form properly under the processing conditions used.

The optical properties of the materials directly influenced the results of the topography measurements; and therefore, it was only possible to obtain these data for samples containing CNTs. The pure PLA/PHBV and CNC-containing samples are transparent in the visible region, with refractive indices ranging from approximately 1.44–1.50 between 300 and 1300 nm and absorption coefficients below 0.12, which characterizes them as low-absorption, high-transmission polymers [15]. Therefore, the optical contrast provided by these surfaces is insufficient for digital optical microscopy, which prevents reliable detection of topography measurements. Samples containing CNTs, in turn, exhibit extraordinary broadband optical absorption and extremely low

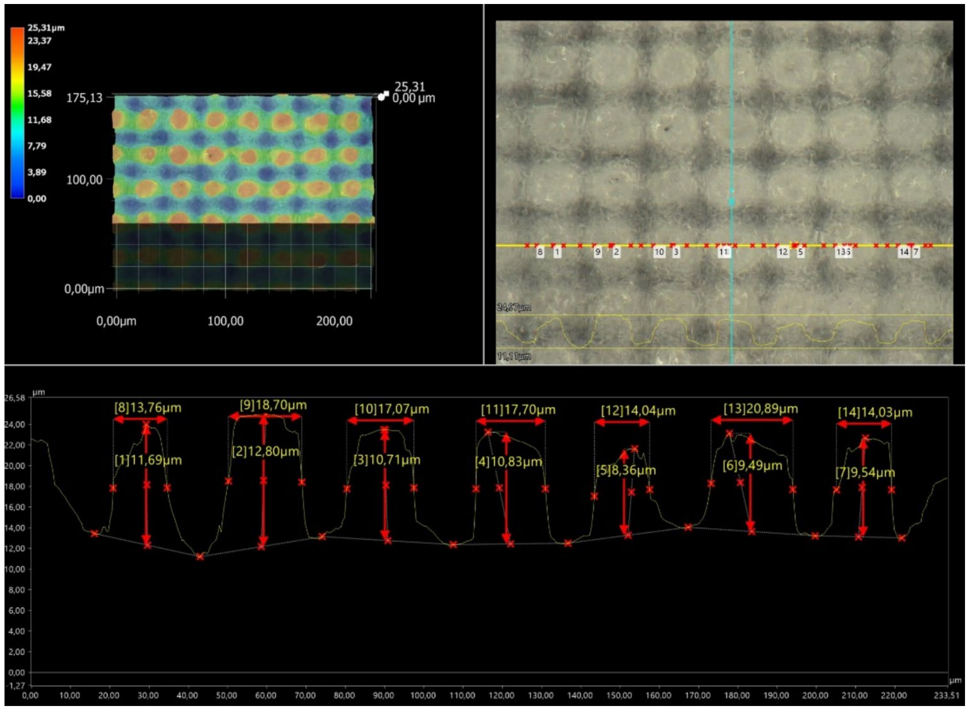

Figure 3 Horizontal line showing the height and width profile of the pillars in the laser-textured PLA/PHBV 80:20 0.5% CNT sample.

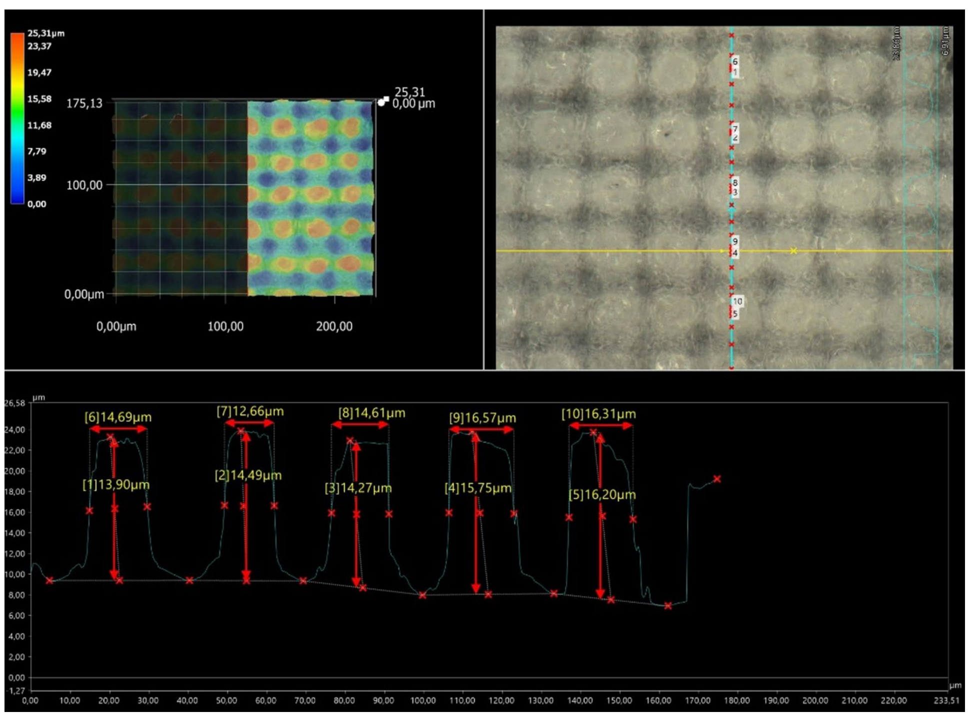

Figure 4 Vertical line showing the height and width profile of the pillars in the laser-textured PLA/PHBV 80:20 0.5% CNT sample.

reflectance. Recent studies [16] have reported CNT-based coatings with reflectance values as low as 2–3% in the visible and NIR regions, and vertically aligned CNT forests can achieve reflectance as low as 0.045%, behaving as near-perfect black absorbers.

Contact angle measurements

The contact angle was measured for all the samples, and the values are shown in Table 3.

Table 2 Topography measurements of the pillar structures for the samples containing different amounts of CNT

Sample	Avg. Height (μm)	Max. Height (μm)	Min. Height (μm)	Avg. Width (μm)	Max. Width (μm)	Min. Width (μm)
PLA/PHBV 80:20 0,5% CNT (horizontal)	10 ± 1	12.8	8.36	16 ± 2	20.89	13.76
PLA/PHBV 80:20 0,5% CNT (vertical)	14 ± 1	16.20	13.90	14 ± 1	16.57	12.66
PLA/PHBV 80:20 1,0% CNT (horizontal)	8 ± 1	10.34	6.82	16 ± 2	19.25	12.44
PLA/PHBV 80:20 1,0% CNT (vertical)	12 ± 2	14.65	8,4	16 ± 1	18.21	13.57
PLA/PHBV 80:20 1,5% CNT (horizontal)						
PLA/PHBV 80:20 1,5% CNT (vertical)	12 ± 1	13.08	11.61	15 ± 1	16.53	12.46
PLA/PHBV 80:20 2,0% CNT (horizontal)						
PLA/PHBV 80:20 2,0% CNT (vertical)	15 ± 2	17.41	11.94	18 ± 3	21.34	15.42

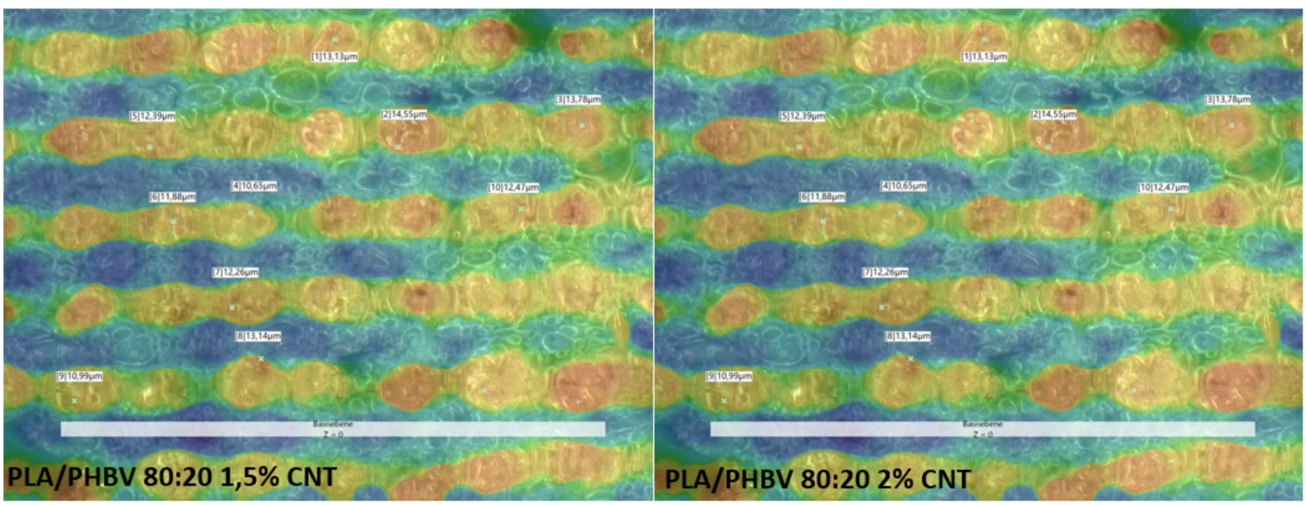

Figure 5 Images obtained by optical profilometry of the samples containing 1.5 and 2% CNT.

Table 3 Contact angle measurements for all samples, laser-treated and untreated

Sample	Contact angle—average and standard deviation (°) - before laser treatment	Contact angle—average and standard deviation (°) - after laser treatment
PHBV	65 ± 0.2	116 ± 0.1
PHBV 1% CNC	78 ± 0.2	104 ± 0.1
PHBV 5% CNC	74 ± 0.1	95 ± 1.8
PHBV 10% CNC	72 ± 0.2	101 ± 0.5
PLA	79 ± 0.1	120 ± 0.1
PLA/PHBV 50:50	84 ± 0.1	121 ± 0.0
PLA/PHBV 60:40	81 ± 0.1	124 ± 0.6
PLA/PHBV 70:30	89 ± 0.6	130 ± 0.0
PLA/PHBV 90:10	89 ± 0.1	128 ± 0.1
PLA/PHBV 80:20 0,5% CNT	75 ± 0.1	107 ± 0.0
PLA/PHBV 80:20 1% CNT	73 ± 0.3	104 ± 0.2
PLA/PHBV 80:20 1,5% CNT	77 ± 0.2	95 ± 0.1
PLA/PHBV 80:20 2% CNT	73 ± 0.3	108 ± 0.2

As can be seen in Table 3, the contact angle increases considerably for all the materials after laser treatment, revealing that they had a more hydrophobic character after the treatment. The changes in the wettability of the samples after laser treatment can be explained based on the Wenzel model [17]. This model describes how surface roughness can influence the contact angle of water. The formula that represents this model is shown in Eq. 1, where θ represents the contact angle of the surface, and r represents the roughness factor.

$$\cos\theta_w = r.\cos\theta \quad (1)$$

According to Eq. 1, the rougher the surface, the greater the contact angle and consequently the more hydrophobic it becomes. After creating a texture with the laser, the roughness of the surfaces is consequently greater, which makes the surface hydrophobic. Fig. 6 shows the behavior of the water droplet on the surface before and after laser treatment, represented by the example of the PLA-PHBV 90:10 sample, which changed its contact angle from 88.55 to 127.56° after laser treatment.

Comparing Fig. 6 with the data in Table 2, it is possible to note that the laser texturing directly affects the wettability of the material, which corroborates the literature proving that femtosecond laser processing has major effects on surface morphology and wettability, and that cell behavior is closely related to surface wettability [18, 19].

Cell viability assay

Viability of L929 cells incubated for 24h on the samples was measured by MTT assay. In order to evaluate the effect of laser texturing on the cell growth, cell viability was calculated by using the values of viability of cells incubated on non-textured samples as control (100% of viability). These results are shown in Fig. 7. In addition, in order to compare the effect of samples composition, the viability of cells was also calculated by using the viability of cells incubated in the absence of samples as 100% of viability (Fig. 8).

According to Figs 7A and 8A, it can be seen that the laser-treated PLA with PHBV contains greater cell viability than before laser treatment, as they all have more than 100% cell viability, except PLA/PHBV 60:40. Although this upward trend was consistent across the PLA/PHBV blends, only the increase observed for pure PLA after laser treatment reached statistical significance when compared to the control group of cells incubated in the absence of samples (Fig. 8A, $p < 0.05$); the relative increases observed among the PLA/PHBV blends themselves (Fig. 7A) did not reach statistical significance, most likely reflecting the variability inherent to the replicates rather than the absence of a biological effect. This means that laser texturing promoted better cell growth, which can be explained by the increased surface area of the material and also because laser structuring leads to the guided growth of cell clusters [19]. One possible explanation for PLA/PHBV 60:40 having lower cell viability after laser texturing may be that this sample also has higher hydrophilicity prior to texturing, as observed according to contact angle measurements. This higher hydrophilicity may have altered the adsorption and conformation profile of serum proteins, creating a surface that did not favor L929 anchoring and spreading. This is because hydrophobic surfaces tend to adsorb fibronectin and albumin in a conformation that favors adhesion; thus, more hydrophilic surfaces may lead to decreased adsorption of adhesion proteins [20].

According to Fig. 7B, PHBV alone had lower cell viability when treated with a laser, but viability increased when CNCs were added. CNCs improve

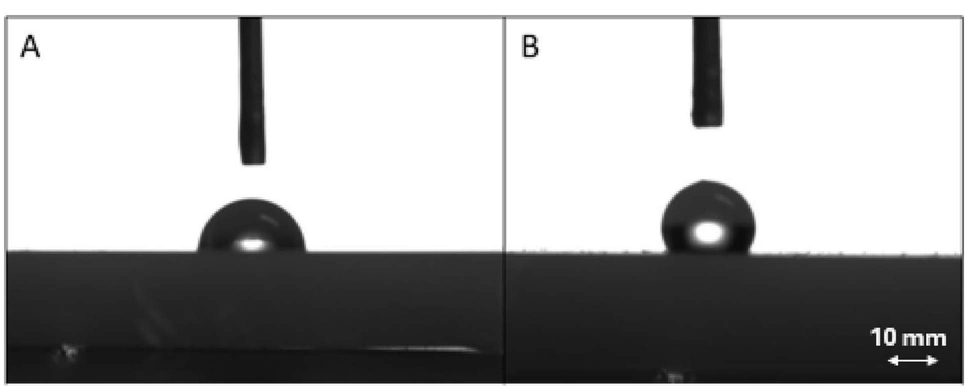

Figure 6 Contact angle to the sample PLA-PHBV 90:10 **a** before and **b** after laser treatment.

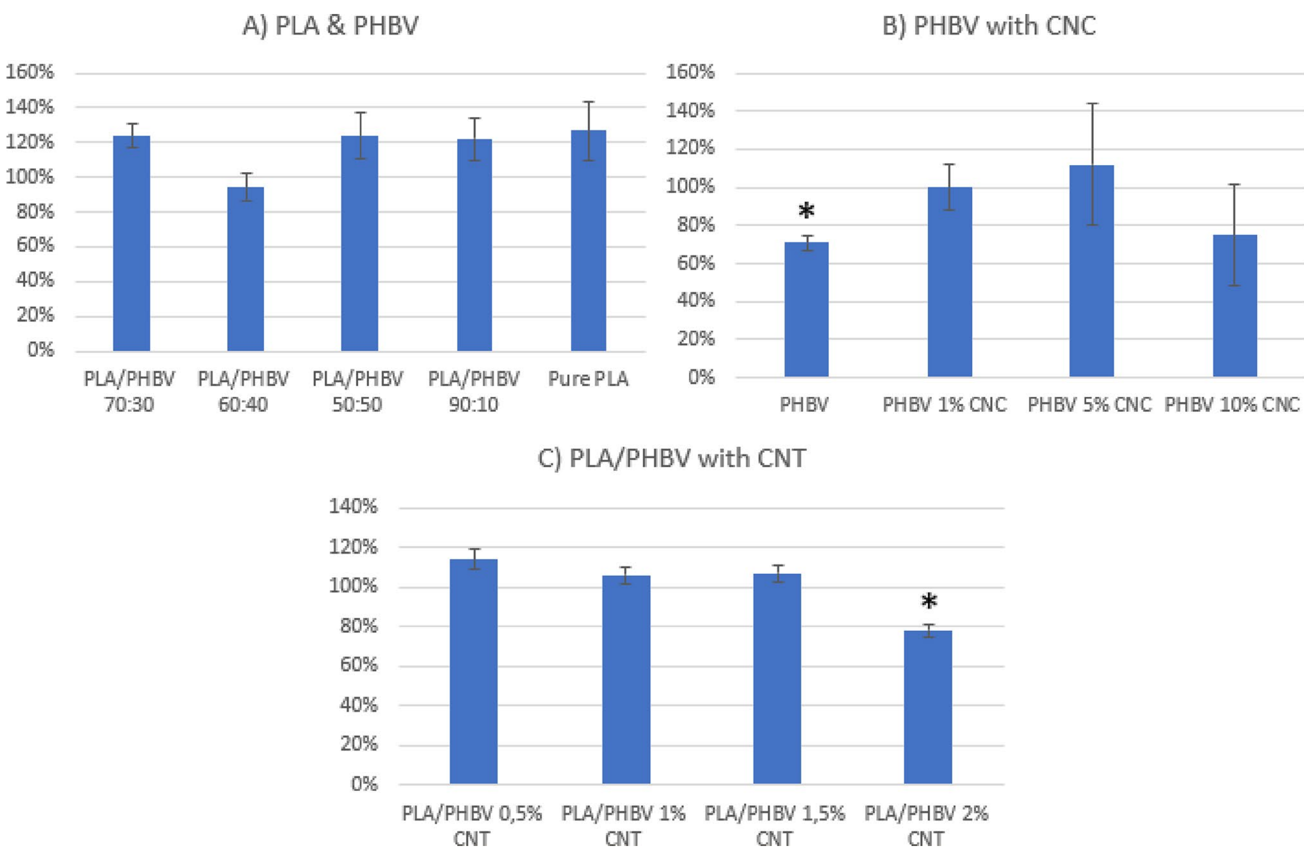

Figure 7 Cell viability test of the L929 cells incubated with different samples for 24h. A) PLA with PHBV at different proportions. B) PHBV with different amounts of CNC. C) PLA/PHBV with different amounts of CNT. Statistical significance is indicated by * ($p < 0.05$), one-sample Student's t-test against the non-laser-treated condition of each material (100%), Bonferroni-corrected.

the thermal stability of the polymer matrix, which can enhance material integrity under treatment, helping explain why low to moderate CNC contents increased viability [21]. However, when the amount of CNC is increased to 10%, cell viability decreases again, revealing that there is an ideal limit where CNCs stop promoting cell viability. Some studies report that, despite the low toxicity of CNCs, depending on the amount, they can cause some toxic results [22]. Even so, the surface charge of the CNC plays an important role in cell adhesion [23]. Furthermore, Fig. 8B clearly shows that the laser did not promote cell growth only when there was 5% CNC in the composition, demonstrating that among the concentrations studied, the one that showed the best results contained 5% CNC. Statistically, however, only PHBV alone (without CNC) showed a significant reduction in viability relative to its own non-laser-treated condition (Fig. 7B, $p < 0.05$), while the formulation containing 1% CNC was the only condition—with and without laser treatment—that differed significantly from the no-material control in the normalized dataset (Fig. 8B, $p < 0.05$). This indicates that, although 5% CNC produced the numerically highest viability among the laser-treated samples, the statistically robust effect within the concentration range tested was observed at the lowest CNC content evaluated (1%), reinforcing the idea that a relatively low CNC loading favors cell viability more consistently than higher concentrations.

By increasing the concentration, there is a possibility that CNC percolation has occurred, where the particles change the mechanical properties of the polymer and make it more rigid, directly affecting cell growth. Finally, CNC above the percolation threshold tends to clump together, forming microgels that can hinder cells' access to the nutrients and oxygen that would keep them alive and growing healthily [24].

Finally, according to Fig. 7C, the CNT-containing material also has greater cell viability when treated with a laser, and in fact, it is reported that the presence

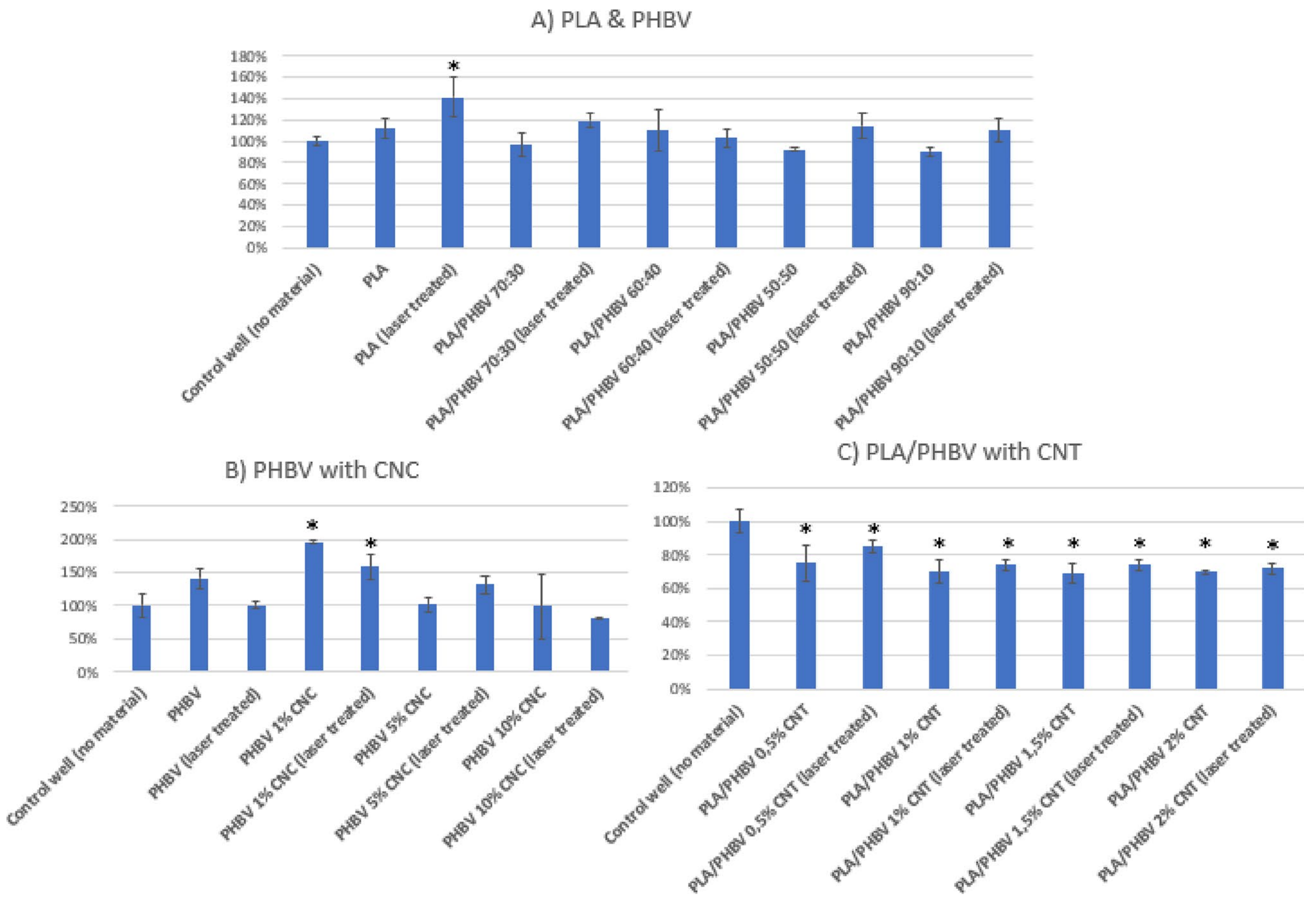

Figure 8 Cell viability of L929 cells, calculated by normalizing the absorbance of each sample by its respective well area, and expressing the result as a percentage relative to the control (no sample). A) PLA with PHBV in different proportions. B) PHBV with different percentages of CNC. C) PLA/PHBV with different percentages of CNT. Statistical significance is indicated by * ($p < 0.05$) relative to the no-material control well, one-way ANOVA followed by a Bonferroni-corrected t test based on the pooled ANOVA variance.

of CNTs has several benefits that promote cell growth [25]. However, when the percentage increases to 2% CNT, it also proves that there is an ideal limit where CNTs stop promoting viability. This is supported by the statistical analysis: comparing each CNT-containing formulation to its own non-laser-treated condition, only the 2% CNT group showed a significant decrease in viability (Fig. 7C, $p < 0.05$), confirming 2% as the concentration at which the beneficial effect of CNT incorporation on cell viability is lost. According to Fig. 8C, cell viability is lower than that of the control in all cases, and there is no significant difference between laser-treated and untreated samples. Indeed, statistical analysis confirmed that all CNT-containing formulations, whether laser-treated or not, differed significantly from the control ($p < 0.05$ for all comparisons), reinforcing that CNT incorporation reduced cell viability across the entire concentration range tested, independently of laser texturing. Studies [26] have shown that percolating networks of carbon nanotubes begin to form at concentrations as low as 0.1%, affecting mechanical and electrical properties. Furthermore, according to the literature [27], non-functionalized CNTs cause significant toxicity via oxidative stress, aggregation, and structural effects on cells. Even so, cell viability percentages are not below 70%, so they did not show significant toxicity to cells, despite the decrease in biocompatibility.

Confocal microscopy

The images obtained by confocal microscopy of cells grown for 24 hours on the samples are shown in Figs 9, 10, 11 and 12.

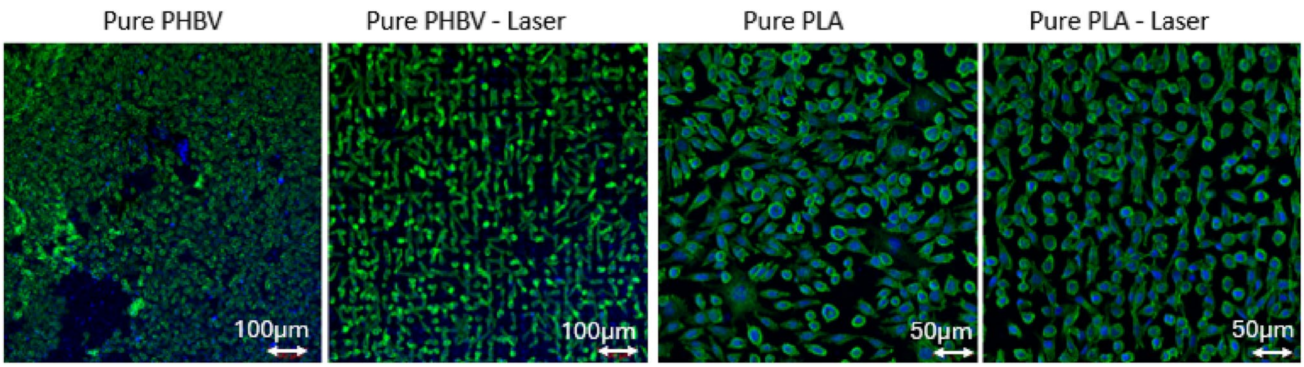

Figure 9 Cells grown for 24 hours on PHBV and pure PLA samples.

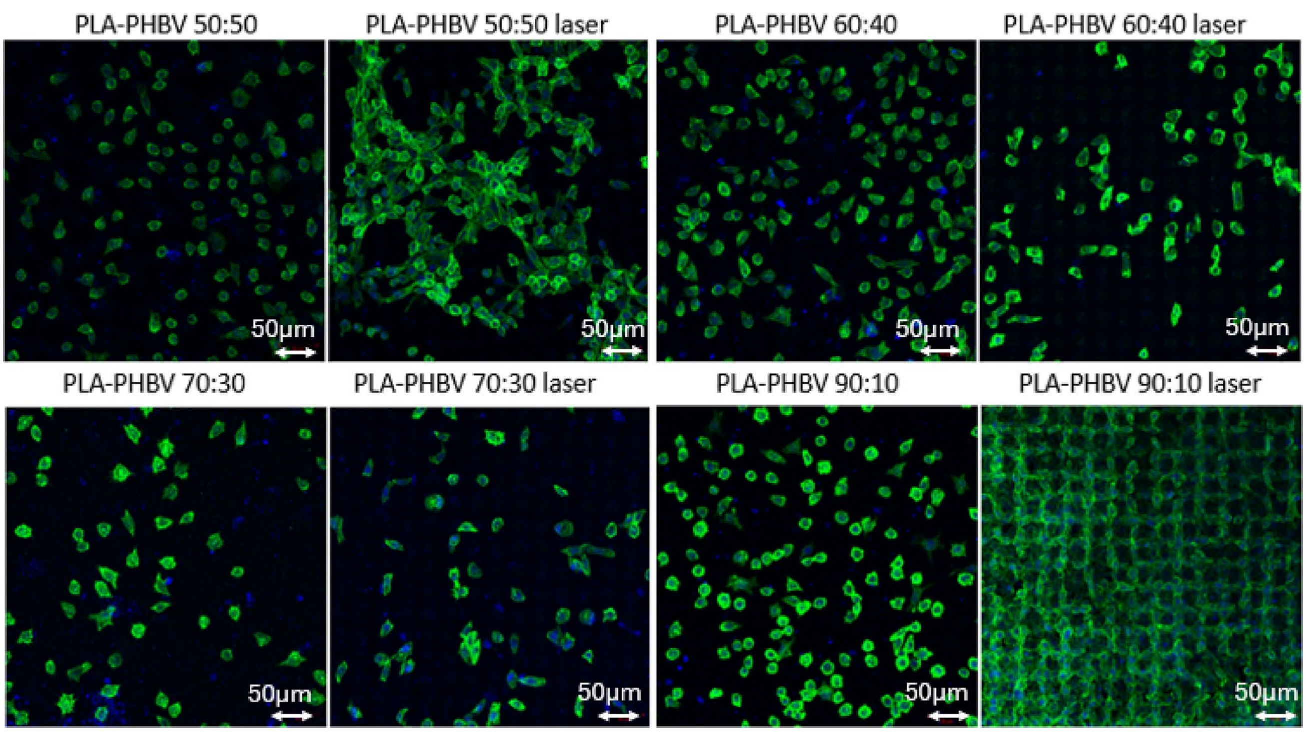

Figure 10 Cells grown for 24 hours on PLA and PHBV samples in different proportions.

For all the samples in Figs 9, 10, 11, and 12, it can be seen that laser texturing promotes directional cell growth when compared to growth in samples without texturing. The directional growth of cells on textured surfaces is reported by Jun et al [19], and Qiu et al [28], where the direction of the pattern directly affects cell proliferation, favoring cell adhesion and differentiation.

The tendency of cell orientation also remains for growth during 48 hours, as shown in Figs 13, 14, and 15.

Jun et al. [19] describe how the formation of micro- and nanostructures using femtosecond lasers influences surface properties such as crystallinity and wettability, which modulate cellular responses. It has been reported that, especially in biodegradable polymers such as PLLA and PLGA, laser-induced periodic surface structures (LIPSS) and microchannels promote cell alignment and the orientation of their spatial distribution, which is directly related to the greater biocompatibility of the material. In addition, Qiu et al. [28] also investigated this behavior using 3D

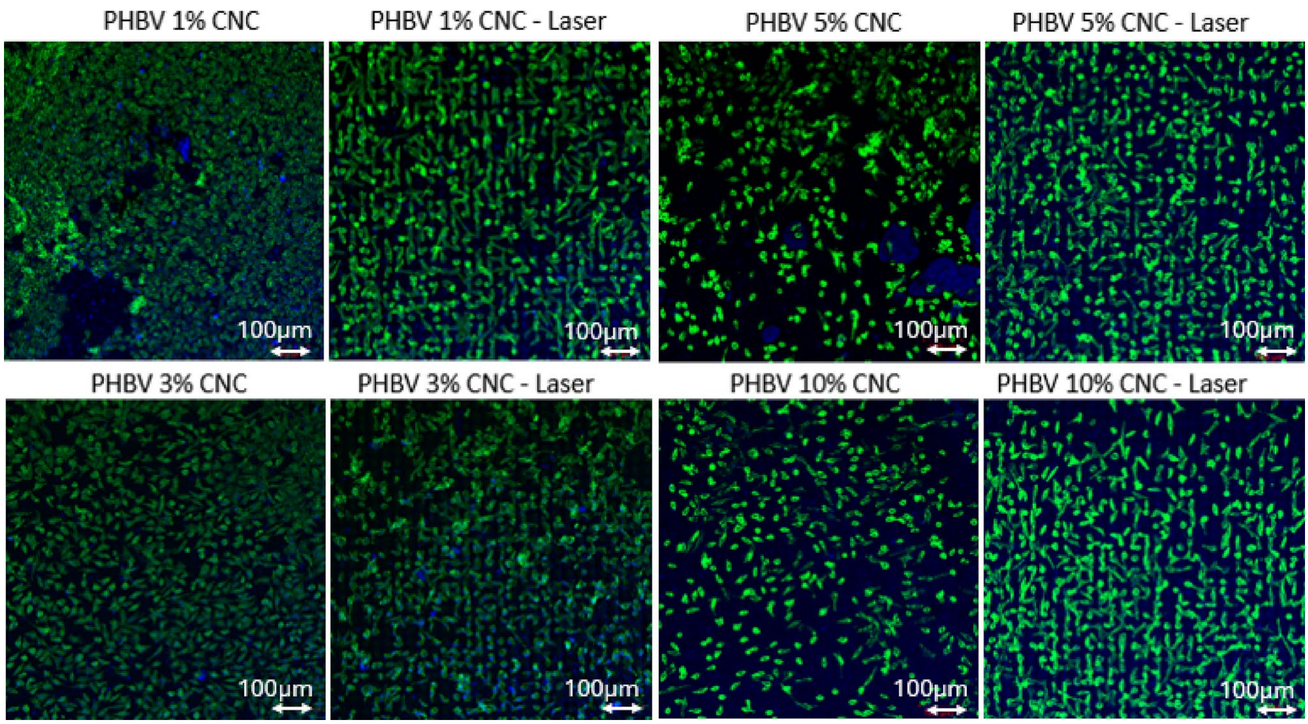

Figure 11 Cells grown for 24 hours on PHBV samples with different concentrations of CNC.

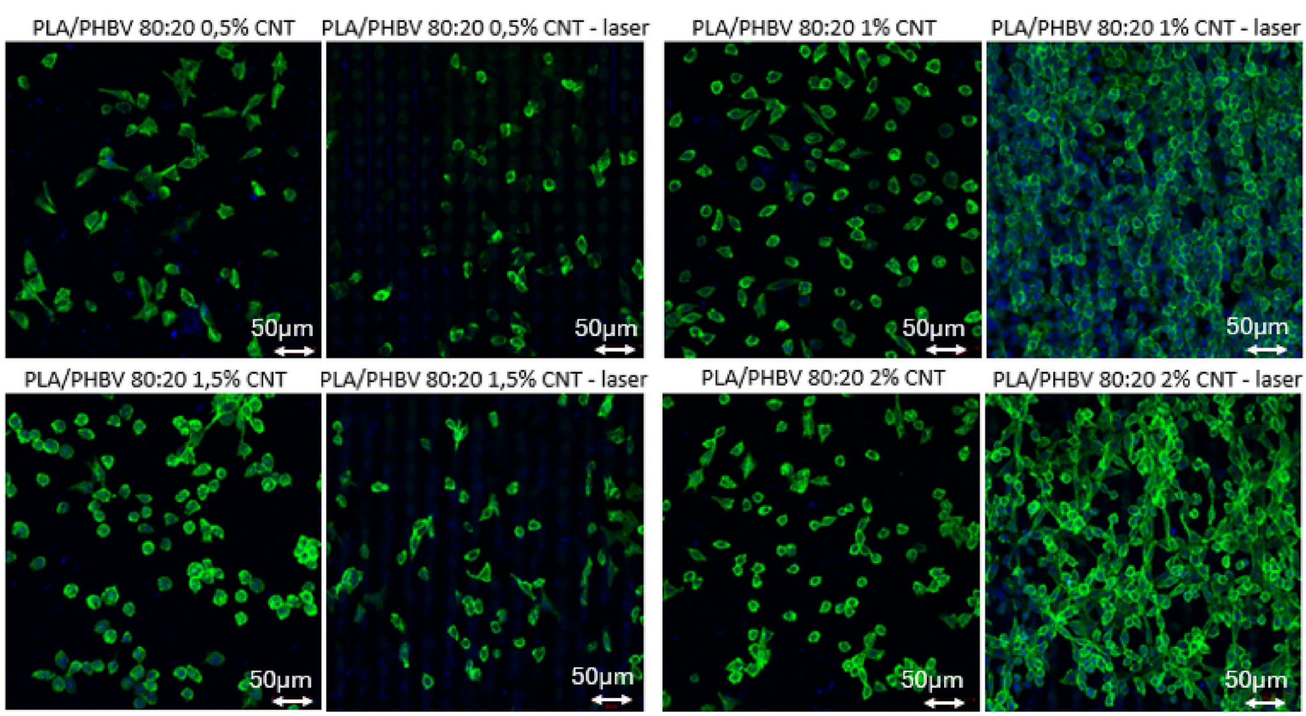

Figure 12 Cells grown for 24 hours on PLA/PHBV samples with different concentrations of CNT.

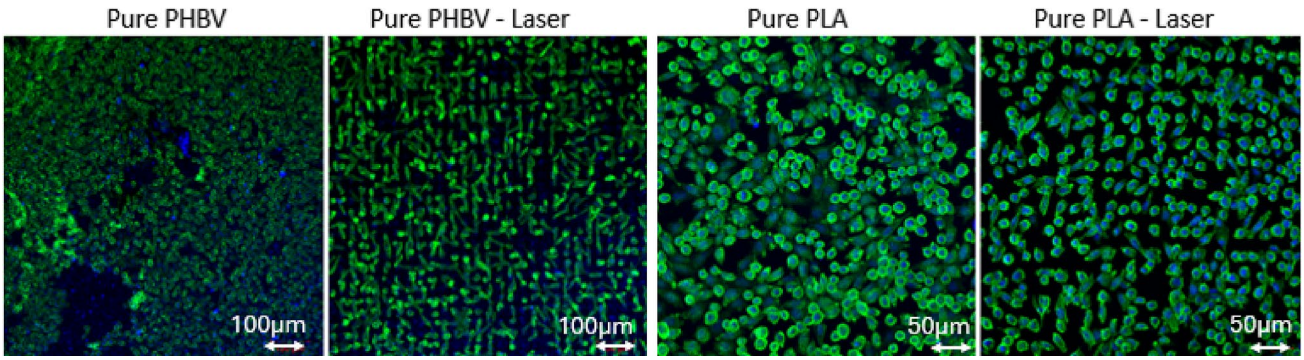

Figure 13 Cells grown for 48 hours on PHBV and pure PLA samples.

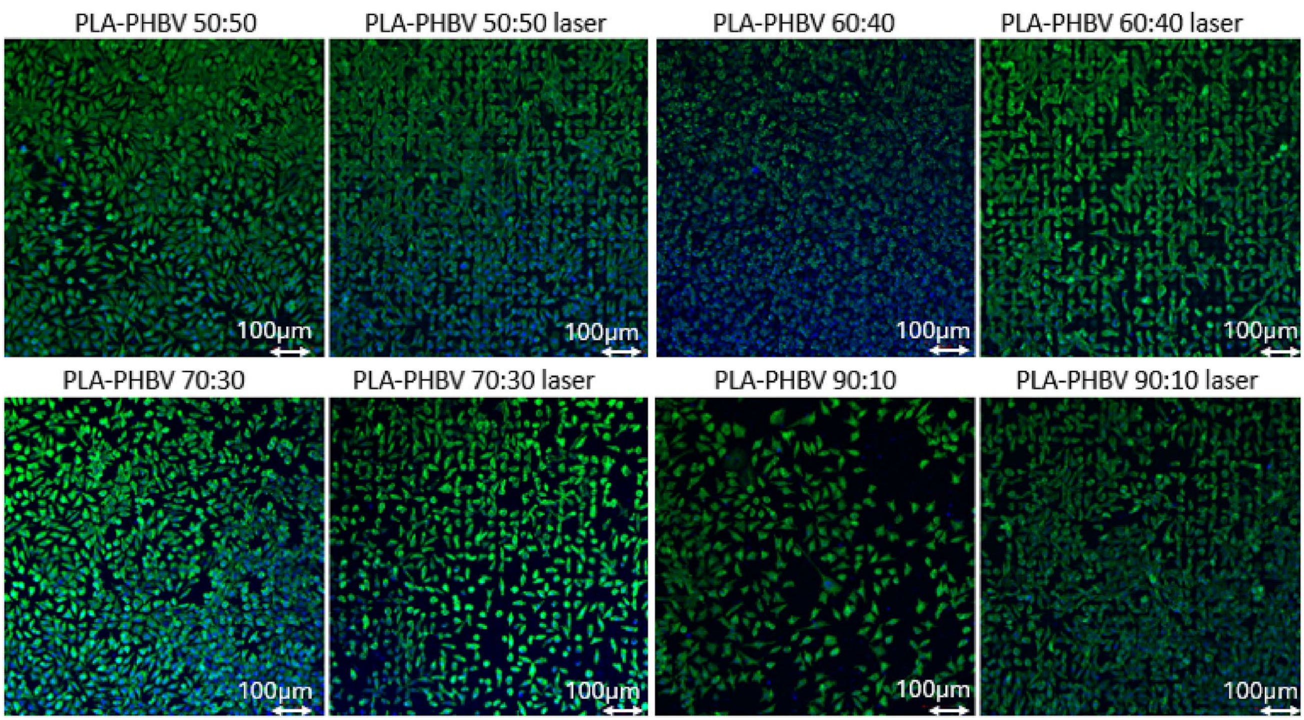

Figure 14 Cells grown for 48 hours on PLA and PHBV samples in different proportions.

microtubes fabricated by femtosecond laser multiphoton polymerization. Neurons cultured on laser-structured microtube arrays showed a significant increase in synaptic differentiation, reaching up to 9 synapses per neuron with lengths of up to 10 µm, in addition to growing along the orientation of the microtubes. This highlights the potential of laser-fabricated architectures to induce highly ordered and functional cell networks.

Finally, when comparing the effect of cell culture time on PLA (Fig. 16), no significant difference in cell growth is observed.

It can be observed, according to Fig. 16, that both at 24 and 48 hours of cell growth on PLA, the levels of cell adhesion and spreading remain similar, with no significant difference in morphology or even in the number of cells. This leads to the understanding that most of the adhesion process probably occurs in the first 24 hours. Qiu et al. [28] report this cell behavior, describing that cells tend to reach a proliferation plateau within 24 hours, especially on two-dimensional surfaces and non-porous structures, due to spatial limitations and reduced nutrient diffusion. Thus, the absence of striking visual differences after 48 hours

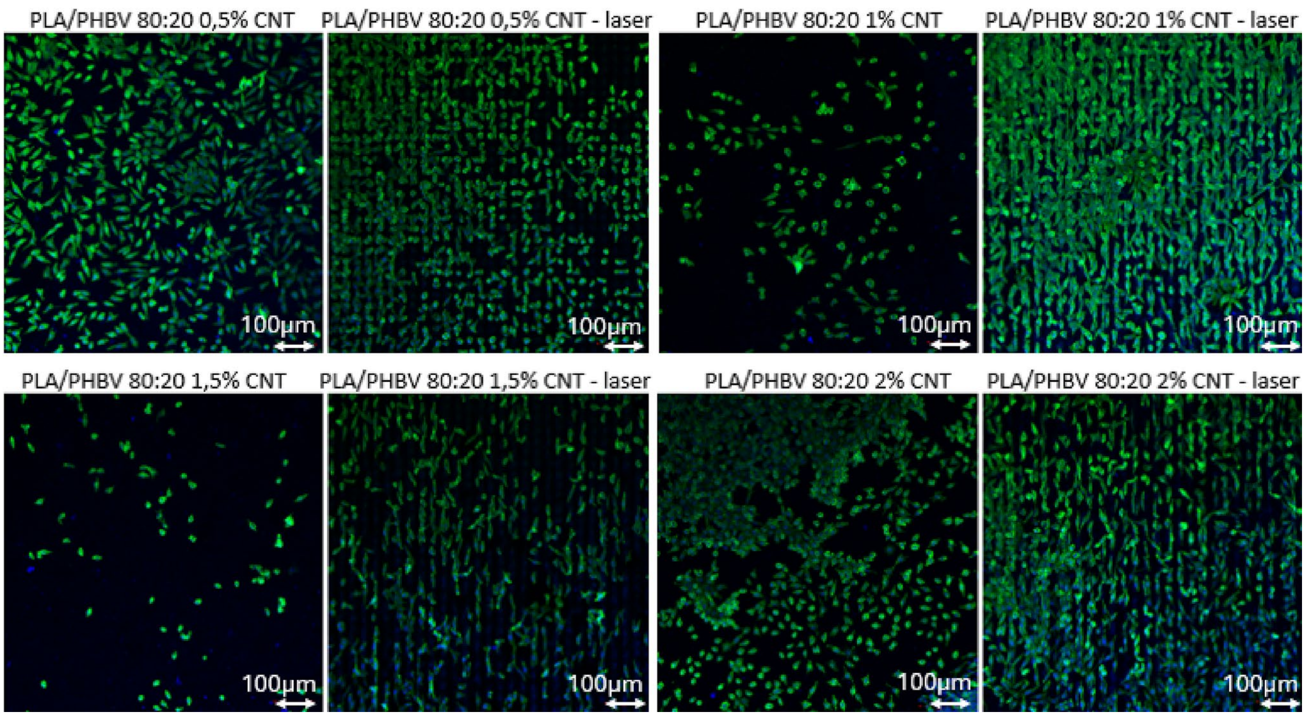

Figure 15 Cells grown for 48 hours on PLA/PHBV samples with different concentrations of CNT.

may be related to the saturation of the area available for new adhesions and the depletion of stimuli favorable to cell spreading.

Conclusion

Based on this study, it can be concluded that the combination of femtosecond laser texturing with the incorporation of nanomaterials into PLA/PHBV polymers does indeed lead to a significant improvement in cellular interactions, making the materials more biocompatible and promoting directional cell growth. Consequently, this reinforces their potential use in biomedical implants, given that the laser-formed micro-pillar structures increased roughness and induced a change in the wettability behavior of the surfaces, directly influencing cell adhesion and proliferation. Among the compositions tested, PLA/PHBV functionalized with 1 wt% CNC showed the most statistically robust improvement in cell viability relative to the no-material control. In contrast, incorporation of CNTs significantly reduced cell viability relative to the control across the entire concentration range evaluated (0.5–2 wt%), regardless of laser texturing, although viability remained above 70% in all CNT-containing formulations, a level generally not associated with significant cytotoxicity. These results highlight the need to further optimize the type and concentration of nanomaterial used in order to maximize biocompatibility. These findings contribute significantly to the development of new-generation biomaterials that combine mechanical strength, biocompatibility, and antibacterial potential, aiming at better clinical results in implants and tissue engineering.

Figure 16 Confocal microscopy of growths on the PLA sample at 24 and 48 hours.

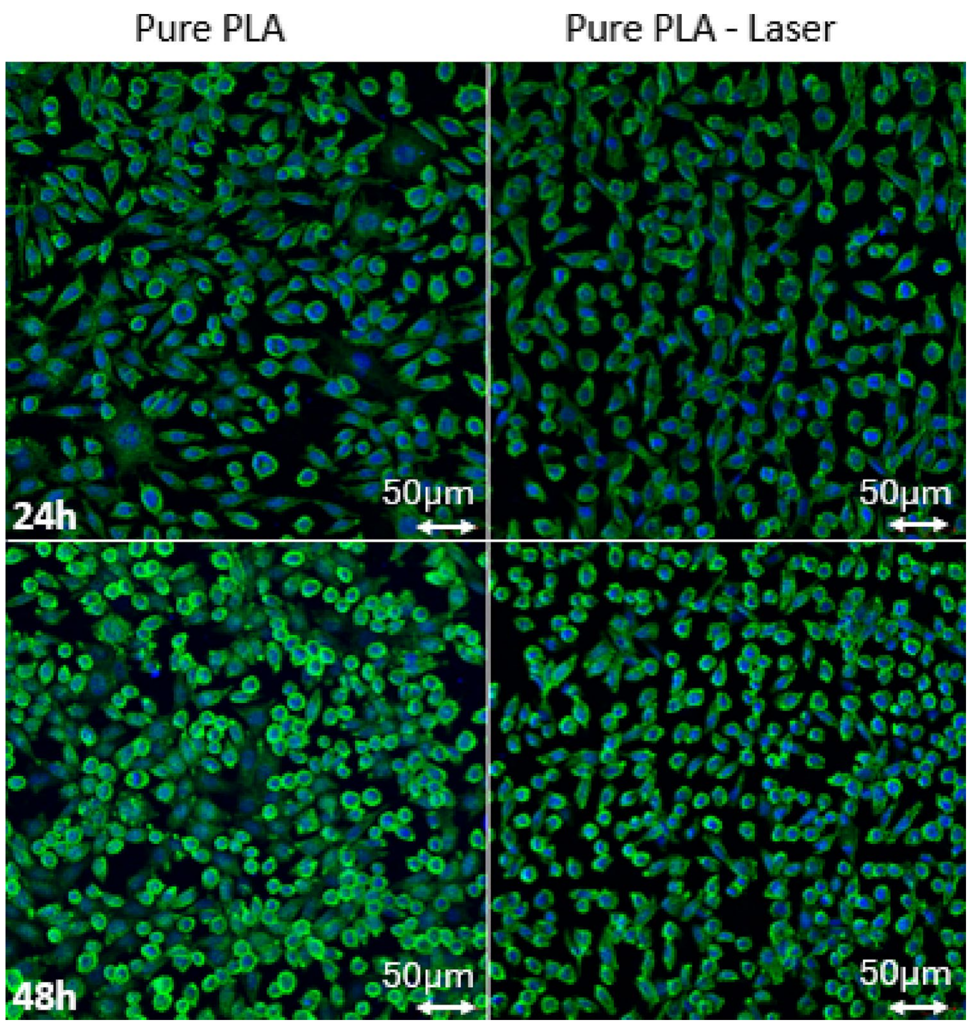

Acknowledgement

This study was financed by the São Paulo Research Foundation (FAPESP), Brazil. Process Number 2021/04838-5; 2023/15972-0. Coordenação de Aperfeiçoamento de Pessoal de Nível Superior - CAPES - colaboration project with German Academic Exchange Service (DAAD) - Process Number 88881.627981/2021-01

Funding

The Article Processing Charge (APC) for the publication of this research was funded by the Coordenação de Aperfeiçoamento de Pessoal de Nível Superior - Brasil (CAPES) (ROR identifier: 00x0ma614). FAPESP, 2023/15972-0, Rafaela Campos Queiroz

References

[1] Celesti C, Gervasi T, Cicero N, Giofrè SV, Espro C, Piperopoulos E et al (2022) Titanium surface modification for implantable medical devices with anti-bacterial adhesion properties. Materials (Basel) 15(9):3283. https://doi.org/10.3390/ma15093283

[2] Lee C, Mayer E, Bernthal N, Wenke J, O'Toole RV (2023) Orthopaedic infections: what have we learned? OTA Int 6(2S):e250. https://doi.org/10.1097/OI9.0000000000000250

[3] Fais LMG, Leite LS, dos Reis BA, Ribeiro ALR, Vaz LG, Klein MI (2021) Microbial adhesion and biofilm formation on bioactive surfaces of Ti-35Nb-7Zr-5Ta alloy created by anodization. Microorganisms 9(10):2154. https://doi.org/10.3390/microorganisms9102154

[4] Rodríguez Á, Trueba P, Amado JM, Tobar MJ, Giner M, Amigó V et al (2020) Surface modification of porous titanium discs using femtosecond laser structuring. Metals (Basel) 10(6):748. https://doi.org/10.3390/met10060748

[5] Lu L, Zhang J, Guan K, Zhou J, Yuan F, Guan Y (2022) Artificial neural network for cytocompatibility and antibacterial enhancement induced by femtosecond laser micro/nano structures. J Nanobiotechnol 20(365):1–17. https://doi.org/10.1186/s12951-022-01578-4

[6] Trebuňová M, Petroušková P, Balogová AF, Ižaríková G, Horňak P, Bačenková D et al (2023) Evaluation of biocompatibility of PLA/PHB/TPS polymer scaffolds with different additives of ATBC and OLA plasticizers. J Funct Biomater 14(8):412. https://doi.org/10.3390/jfb14080412

[7] Pan W, Xiao X, Li J, Deng S, Shan Q, Yue Y et al (2018) The comparison of biocompatibility and osteoinductivity between multi-walled and single-walled carbon nanotube/PHBV composites. J Mater Sci Mater Med 29(189):1–14. https://doi.org/10.1007/s10856-018-6197-3

[8] Bazan P, Rochman A, Mroczka K, Badura K, Melnychuk M, Nosal P et al (2024) Composites based on PLA/PHBV blends with nanocrystalline cellulose NCC: mechanical and thermal investigation. Materials 17(24):6036. https://doi.org/10.3390/ma17246036

[9] Rakebrandt JH, Zheng Y, Besser H, Scharnweber T, Seifert HJ, Pfleging W (2020) Laser-assisted surface processing for functionalization of polymers on micro- and nano-scale. Microsyst Technol 26:1085–1091. https://doi.org/10.1007/s00542-019-04633-7

[10] Silva APB, Montagna LS, Passador FR, Rezende MC, Lemes AP (2021) Biodegradable nanocomposites based on PLA/PHBV blend reinforced with carbon nanotubes with potential for electrical and electromagnetic applications. Express Polym Lett 15:987–1003. https://doi.org/10.3144/expresspolymlett.2021.79

[11] Gerard T, Budtova T, Podshivalov A, Bronnikov S (2014) Polylactide/poly(hydroxybutyrate-co-hydroxyvalerate) blends: morphology and mechanical properties. Express Polym Lett 8:609–617. https://doi.org/10.3144/expresspolymlett.2014.64

[12] Oyama IMC, dos Anjos EGR, Morgado GFM, Martins EF, Passador FR (2023) Antistatic and antimicrobial packaging of PLA/PHBV blend-based graphene nanoplatelets nanocomposites. J Appl Polym Sci 140(40):e54484. https://doi.org/10.1002/app.54484

[13] Obilor AF, Pacella M, Wilson A, Silverschmidt VV (2022) Micro-texturing of polymer surfaces using lasers: a review. Int J Adv Manuf Technol 120:103–135. https://doi.org/10.1007/s00170-022-08731-1

[14] Wang H, Deng D, Zhai Z, Yao Y (2024) Laser-processed functional surface structures for multi-functional applications-a review. J Manuf Process 116:247–283. https://doi.org/10.1016/j.jmapro.2024.02.062

[15] Amendola C, Lacerenza M, Pirovano I, Contini D, Spinelli L, Cubeddu R et al (2021) Optical characterization of 3D printed PLA and ABS filaments for diffuse optics applications. PLoS ONE 16(6):e0253181. https://doi.org/10.1371/journal.pone.0253181

[16] Saini S, Reshmi S, Gouda GM, Kumar SA, Sriram KV, Bhattacharjee K (2021) Low reflectance of carbon nanotube and nanoscroll-based thin film coatings: a case study. Nanoscale Adv. 3(11):3184–3198. https://doi.org/10.1039/d0na01058h

[17] Kunz C, Müller FA, Gräf S (2018) Multifunctional hierarchical surface structures by femtosecond laser processing. Materials (Basel) 11(5):789. https://doi.org/10.3390/ma11050789

[18] Toosi S, Maradi S, Hatzikiriakos SG (2017) Fabrication of micro/nano patterns on polymeric substrates using laser ablation methods to control wettability behavior: a critical review. Rev Adhes Adhes 5:55–78. https://doi.org/10.1002/9781119526445.ch2

[19] Jun I, Chung YW, Heo YH, Han HS, Park J, Jeong H et al (2016) Creating hierarchical topographies on fibrous platforms using femtosecond laser ablation for directing myoblasts behavior. ACS Appl Mater Interfaces 8(5):3407–3417. https://doi.org/10.1021/acsami.5b11418

[20] Webb K, Hlady V, Tresco PA (1998) Relative importance of surface wettability and charged functional groups on NIH 3T3 fibroblast attachment, spreading, and cytoskeletal organization. J Biomed Mater Res 41(3):422–430. https://doi.org/10.1002/(sici)1097-4636(19980905)41:3%3c422::aid-jbm12%3e3.0.co;2-k

[21] Magnani C, Idström A, Nordstierna L, Müller AJ, Dubois P, Raquez JM et al (2020) Interphase design of cellulose nanocrystals/poly(hydroxybutyrate-ran-valerate) bionanocomposites for mechanical and thermal properties tuning. Biomacromol 21(5):1892–1901. https://doi.org/10.1021/acs.biomac.9b01760

[22] Seabra AB, Bernardes JS, Fávaro WJ, Paula AJ, Durán N (2018) Cellulose nanocrystals as carriers in medicine and their toxicities: a review. Carbohydr Polym 181(1):514–527. https://doi.org/10.1016/j.carbpol.2017.12.014

[23] Mahmoud KA, Mena JA, Male KB, Hrapovic S, Kamen A, Luong JHT (2010) Effect of surface charge on the cellular uptake and cytotoxicity of fluorescent labeled cellulose nanocrystals. ACS Appl Mater Interfaces 2(10):2924–2932. https://doi.org/10.1021/am1006222

[24] Redondo A, Mortensen N, Djeghdi K, Jang D, Ortuso RD, Weder C et al (2022) Comparing percolation and alignment of cellulose nanocrystals for the reinforcement of polyurethane nanocomposites. ACS Appl Mater Interfaces 14(5):7270–7282. https://doi.org/10.1021/acsami.1c21656

[25] Maghimaa M, Sagadevan S, Boojhana E, Fatimah I, Lett JA, Moharana S, Garg S, Anber MA (2024) Enhancing biocompatibility and functionality: carbon nanotube-polymer nanocomposites for improved biomedical applications. J Drug Deliv Sci Technol 99:105958. https://doi.org/10.1016/j.jddst.2024.105958

[26] Lebedev SM (2020) PCL-CNT nanocomposites prepared by melt compounding and evaluation of their basic Properties. Polym Compos 41(5):1830–1840. https://doi.org/10.1002/pc.25501

[27] Chetyrkina MR, Fedorov FS, Nasibulin AG (2022) In vitro toxicity of carbon nanotubes: a systematic review. RSC Adv 12(25):16235–16256. https://doi.org/10.1039/d2ra02519a

[28] Qiu Y, Wang X, Yu H, Zhang Y, Zheng J, Wang J, Gan Q, Liu L, Li WJ (2024) Engineering 3D microenvironments with femtosecond laser-fabricated microtubes to direct neuronal network formation. Addit Manuf 88:102449. https://doi.org/10.1016/j.addma.2024.104249